Grain rotation in impurity-doped two-dimensional colloidal polycrystals

Joseph D. Hutchinson[1,2] and Roel P. A. Dullens[1,3,*]

[1]*Department of Chemistry, Physical and Theoretical Chemistry Laboratory, University of Oxford, South Parks Road, Oxford OX1 3QZ, United Kingdom*

[2]*Center for Systems Biology Dresden, Pfotenhauerstr. 108, 01307 Dresden, Germany*

[3]*Institute for Molecules and Materials, Radboud University, Heyendaalseweg 135, 6525 AJ Nijmegen, The Netherlands*

(Received 21 December 2023; accepted 11 June 2024; published 11 July 2024)

Grain texture evolution and coarsening after quenching can be achieved by curvature-driven growth and grain rotation. Here we examine grain rotation in coarsening, impurity-doped, two-dimensional colloidal polycrystals. We find the rate of rotation to be independent of the impurity concentration and proportional to the inverse of the grain size. The latter is rationalized by considering grain rotation driven by grain-boundary sliding and particle diffusion in the lattice. We also show that rotation driven grain growth and curvature driven growth are independent, with the latter being the dominant mechanism in our system. Next, we examine the dislocation reactions underlying grain rotation and observing its facilitation via the effective "sinking" of grain-boundary dislocations into triple junctions, as has been predicted by simulations.

DOI: 10.1103/PhysRevMaterials.8.075603

I. INTRODUCTION

Rotation at the microscale is often driven by a torque resulting from an energy gradient along the surface of the body; examples being micromotors utilizing interfacial tension gradients [1], cholesteric droplets rotating with a temperature gradient [2], and electrochemical gradients in motor proteins driving the rotation of bacterial flagella [3]. Domain growth in polycrystals is typically driven by a reduction in the total interfacial energy of the system, which generally manifests as curvature-driven grain growth [4]. However, grain rotation is another means of interfacial energy reduction, as grain boundaries (GBs) with smaller misorientations are generally lower in energy with a lower density of dislocations [5]. With sufficient rotation grains can combine, a process known as grain-rotation-induced coalescence [6–8].

Grain rotations can be observed in atomic systems under certain conditions, such as annealing thin films [9,10], materials under strain [11,12], and in the coarsening of alloys and ceramics [13–15]. There have also been numerous simulations studying the rates and incidence of grain rotation during coarsening [16–19]. In particular, Moldovan *et al.* [6] found the angular velocity ω of simulated grains to be well described by $\omega = M\tau$, where $M = CR^{-p}$ is the rotational mobility, R is the radius of the grain, p an integer, C a constant dependent upon the width of the GB, grain size and ratio of particle diffusion constants within the lattice and GB [20], and τ is the torque. In setting out a theory for the mechanism of grain rotation, Li [13] suggested there are two possible rate-controlling processes: the motion of dislocations in the grain boundary and diffusion of particles in the grain. Whichever mechanism is the slowest will determine C and p.

In atomic systems, rotation-induced coalescence is often measured under conditions where the relative contribution of rotation to grain growth is elevated, such as via increased torque through applied stress, or faster particle diffusion at higher temperatures [13,21–23]. For grain growth during typical recrystallization, however, curvature-driven growth can be impeded by the presence of impurities, as Zener pinning lowers the translational mobility of grain boundaries [4]. The mechanism of grain rotation will be affected differently by the presence of impurities, therefore, the relative contribution of grain rotation to grain growth may be different for doped materials. As real materials are likely to contain impurities [5,24], understanding grain rotation is important to help controlling grain size and therefore material properties.

Grain rotation has also been observed in colloidal crystals—which allowed for a detailed analysis of the structure and dynamics at the particle level—during the coalescence of isolated crystallites [7] and the shrinkage of grain-boundary loops [25–27]. However, the latter experiments are not necessarily representative of grain growth in polycrystals, owing to the lack of a grain-boundary network. More recently, grain rotation in colloidal polycrystals under shear was studied [28], finding stress-induced rotation to be permitted by the emission of dislocations from grain boundaries. Additionally, spontaneous grain rotation leading to coalescence has been observed in adjacent grain-boundary loops [29]. Also, the role of impurities in grain-boundary segregation [30] and curvature driven grain growth [31] has been addressed in colloidal crystals containing a controlled amount of impurities. However, the effect of impurities on grain

*Contact author: roel.dullens@ru.nl

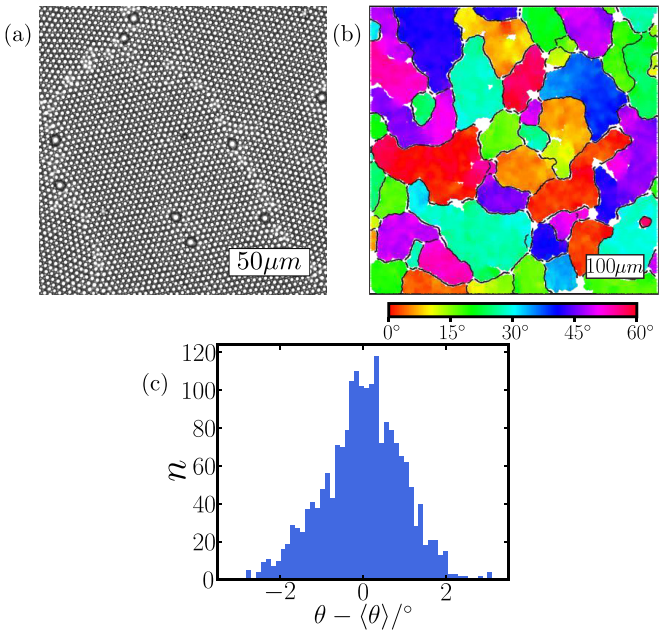

FIG. 1. (a) A representative image of the doped polycrystalline colloidal monolayer. (b) An image showing the grains colored by orientation (see the color bar), and the grain boundaries drawn in black. (c) A distribution of individual particles' orientations within a representative single grain, relative to the average.

rotation in polycrystalline colloidal systems have not been addressed to date. Furthermore, previous work has suggested that triple-junctions may be reaction sites that effectively act as "sinks" for dislocations during grain rotation, which has been observed in simulations [32].

In this work, we measure and examine the role of grain rotation in an impurity-doped polycrystalline monolayer of colloidal particles undergoing grain growth. Note that the roles of crystallization and curvature-induced grain growth were studied in Ref. [31]. Here, we track the rotational velocity of the grains, finding that it is proportional to the inverse of the grain size, with the apparent mechanism consistent with grain sliding [33]. We contextualise the rates of rotation and rotation driven grain growth to the overall rate of coarsening and presence of impurities. We next directly visualize the dislocation dynamics underlying grain rotation, and demonstrate the role of triple junction as an effective "source" and sink of dislocations during grain rotation.

II. EXPERIMENTAL METHODS

The experimental colloidal system is formed by a monolayer of melamine formaldehyde spheres, comprised of host and impurity particles, with diameters of 2.95 μm and 6.20 μm, respectively. The monolayer sits at the bottom of a quartz (20 mm × 9 mm × 200 μm) Hellma cell [25,30,31,34], an example of which can be seen in Fig. 1(a). The total area fraction is $\phi \approx 0.75$, with six impurity concentrations in the range $0 < \phi_i \leqslant 0.114$, and the data are averaged over 42 different experimental runs. Images are taken on an Olympus CKX41 bright-field microscope with an Olympus 20× objective, and a field-of-view encompassing $\approx 3.5 \times 10^4$ particles. Image recording begins concurrent with the sedimentation of particles to the bottom of the cell. The result is a polycrystalline structure which coarsens over time, with grains consisting of neighboring similarly orientated particles, shown in Fig. 1(b). As particles sediment to the bottom of the cell, the system becomes quenched into the crystalline phase and therefore crystallizes. Crystal growth occurs simultaneously with grain boundary driven growth, as was addressed in our previous work [31].

We find particle coordinates using standard procedures [35], and we detect individual grains and the grain boundaries using the methods of Lavergne *et al.* [31,34]. Next, we find all of the particles within a single grain and the segments of the grain boundary, each with a length Λ_j and misorientation $\Delta\theta_j$. A representative distribution of the orientations of the particles, θ, is shown in Fig. 1(c). The grain radius R is approximated using the number of particles, n, in the grain: $R = \frac{1}{2}a_0\sqrt{n}$, where a_0 is the lattice spacing. The orientation of the grain is taken as the average of the distribution, $\langle\theta\rangle$. We measure the angular velocity ω, by measuring the change in $\langle\theta\rangle$ over a time range of $15t_B$ (where $t_B \approx 30$ s). This time range is chosen as the fluctuations in $\langle\theta\rangle$ are found to be uncorrelated after this time lag.

III. RESULTS AND DISCUSSION

A. Quantifying grain rotation in a polycrystal

From our experiments, we determine how the average orientation of the particles in a grain, $\langle\theta\rangle$, changes with time at a rate $\omega = d\langle\theta\rangle/dt$, where ω is the angular velocity. First, we examine the probability distributions of the measured angular velocities in Fig. 2(a) for three different impurity concentrations ϕ_i. Crucially, we examine a narrow window of grain sizes (radii of $4a_0$–$6a_0$) to minimize any size-dependence of the angular velocity. This is important because higher impurity concentrations lead to slower grain growth rates and a smaller average grain size, as shown in our previous work on this system [31]. Interestingly, there is no apparent difference between each ϕ_i, which suggests that the presence of impurities does not affect the grain rotation mechanism. Thus, in the following, we average our data over all ϕ_i. Additionally, the majority of impurities are located in the grain boundaries [30,31], which would sensitively affect the motion of dislocations in the boundaries. Therefore, we anticipate the diffusion of particles in the grain to be the rate-determining mechanism for grain rotation [13].

Next, we quantify the rate of grain rotation. Following Ref. [6], we note that a grain has multiple neighboring grains, each contributing a segment j to the total grain-boundary length, with its own misorientation $\Delta\theta_j$, length Λ_j, and grain-boundary energy γ_j. Each segment will provide a contribution to the total torque based on the magnitude and direction of the energy gradient, and length of the boundary: $\tau = \sum_j \Lambda_j \gamma_j'$, where $\gamma_j' = d\gamma_j/d\Delta\theta_j$, which is positive (negative) if the energy gradient favors clockwise (anticlockwise) rotation [6,9,20]. Using the Read-Shockley equation for grain-boundary energy [36], $\gamma = \gamma_0\Delta\theta(A - \ln\Delta\theta)$, where γ_0 and A

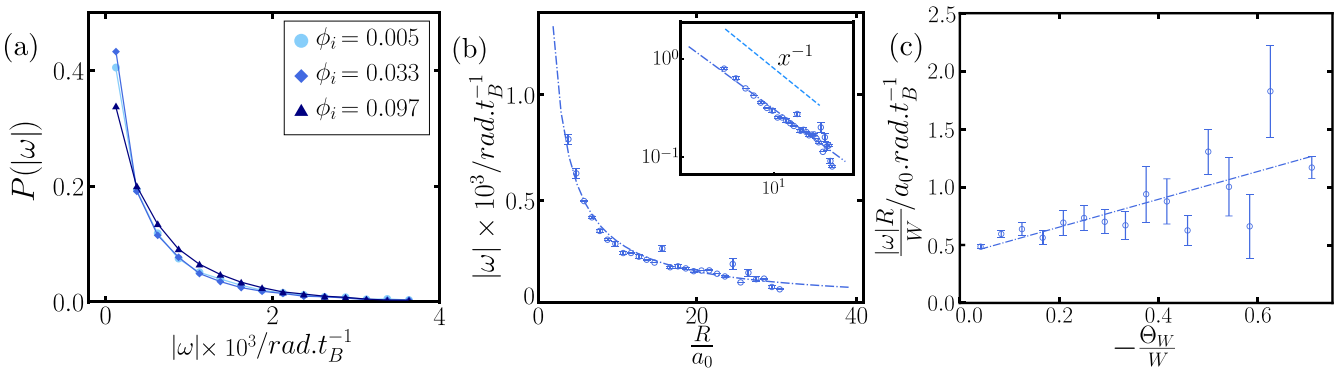

FIG. 2. (a) The distributions of grain angular velocities for three different impurity area fractions, ϕ_i, all taken for a small window of grain sizes ($4a_0$–$6a_0$). (b) A plot of grain radius R, scaled by the lattice spacing a_0 against the magnitude of the angular velocity of each grain, ω, in radians per Brownian time t_B. The inset is the log-log plot of this. (c) The components of Eq. (4) plotted.

are constants, the torque can be expressed as

$$\tau = 2\pi R\gamma_0(A_W - \Theta_W). \tag{1}$$

Here, A_W and Θ_W are the sums over the grain-boundary segments' contributions to the grain-boundary energy gradient, $A_W = \{A-1\}\sum_j s_j\Lambda_j/2\pi R$ and $\Theta_W = \sum_j s_j\Lambda_j \ln\Delta\theta_j/2\pi R$. Note that both A_W and Θ_W are divided by the perimeter of the grain $\sum_j \Lambda_j = 2\pi R$ (assuming circular grains), meaning that both quantities are weighted averages, which are measurable from our experiments.

The direction of the grain boundary energy gradient is encompassed by $s_j = \pm 1$. Recalling that $\omega = M\tau = C\tau R^{-p}$ [6], we can use Eq. (1) to write the angular velocity of a rotating grain as

$$\omega = 2\pi C\gamma_0 \frac{A_W - \Theta_W}{R^{p-1}}. \tag{2}$$

From Eq. (2), we expect a power-law relationship between ω and R. As shown in Fig. 2(b), where we plot $|\omega|$ as a function of the grain size R, we find that ω is almost inversely proportional to R: $|\omega| \sim R^{-k}$, with $k = 0.92$. Intriguingly, this is in contrast with previous analytical and simulation approaches to grain rotation in polycrystalline networks [9,13,37], where the exponent was reported to be all integers from -5 to 0, *excluding* -1.

To rationalize this dependence, similarly to the approach of Moldovan *et al.* [20], we apply Raj and Ashby's theory of diffusion-accommodated grain-boundary sliding [33] to obtain an expression for the angular velocity of grain rotation. As shown in the Appendix, we find the following expression:

$$\omega = \frac{2\tau}{k_BTR^2}D_L, \tag{3}$$

where D_L is the diffusion constant of particles in the lattice. Comparing Eq. (3) with $\omega = M\tau = CR^{-p}\tau$ [6] shows that within this diffusion-accommodated grain-boundary sliding approach [33], $p = 2$ and $C = 2D_L/k_BT$. Therefore, the rotational mobility $M = 2D_L/k_BTR^2$.

As $\omega \propto R^{-(p-1)}$ [see Eq. (2)], this leads to $\omega \propto R^{-1}$, consistent with the exponent measured in our experiments. It is important to note that to obtain Eq. (3) (see Appendix), we deviate from Moldovan *et al.* [20] in two respects. First, we treat the shape of the grain boundary to be independent of the grain size. This is based on our previous work on this system [31], where we found that the system exhibits dynamic scaling. Hence, we expect self-similarity in the grain size and shape and therefore that they are independent. Second, we truncate the Fourier series describing the boundary shape at the first term (see Appendix), as in our colloidal system, any roughness should be averaged out due to thermal fluctuations of the boundary [38]. From the comparison with the diffusion-accommodated grain-boundary sliding approach [33], we thus infer that the grain rotation observed in our experiments are being driven by particle diffusion through the lattice. This is encapsulated in the rotational mobility M, which is dependent upon rate of diffusion D_L and inversely proportional to the number of particles that must diffuse ($M \propto n^{-1}$ as $n \propto R^2$).

Having quantified and uncovered the origin of the grain-size dependence of ω, we can now use Eq. (3) to test if the torque is well described using the Read-Shockley equation, and then determine D_L. From our data, we measure the grain radius R, angular velocity $|\omega|$ and weighted average misorientation Θ_W and A_W. The latter parameter A_W is rewritten as $A_W = \{A-1\}W$, where $W = \sum_j s_j\Lambda_j/2\pi R$. Combining Eqs. (1) and (3) and rearranging, we find:

$$\frac{\omega R}{W} = \frac{4\pi\gamma_0 D_L}{k_BT}\left(\{A-1\} - \frac{\Theta_W}{W}\right). \tag{4}$$

Based on Eq. (4), we plot $\omega R/w$ as a function of $-\Theta_W/W$, as shown in Fig. 2(c), and observe that the data are indeed well described by a linear fit. From the gradient, we can determine D_L, as $\gamma_0 = Ea_0/8\pi(1-\nu^2)$ [36], where E is the Young's modulus, a_0 the lattice spacing, and ν the Poisson ratio. From previous work on colloidal crystals, we use the approximate values of $\nu = 1/3$ [39] and $E = 560k_BT/a_0^2$ [40] and combine this with the measured gradient of $1.20a_0t_B^{-1}$ to find a value of $D_L = 1.1 \times 10^{-3}\ \mu m^2\ s^{-1}$.

Within our experimental time window we did not reach the long-time diffusive limit to be able to reasonably measure D_L directly. Nevertheless, there are experimental studies examining vacancy diffusion albeit in very soft colloidal crystals [41] where the vacancies are delocalized, resulting in high diffusivity [42]. For hard-sphere potentials, simulations show that vacancy diffusivity decreases with an increased area fraction

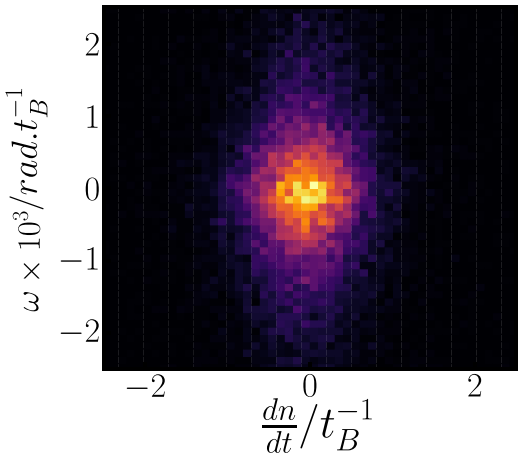

FIG. 3. A 2D histogram of the change in the number of particles in a grain, dn/dt, versus the angular velocity, ω. Note that the quantities have been averaged over $10t_B$ to reduce noise.

to become one or two orders of magnitude slower than that of a single particle [43,44]. As we are not aware of experimental measurements of lattice diffusion in the literature, we rationalize the value of D_L, by considering lattice diffusion as the activated motion of particles mediated by an activation energy E_a, in line with previous theoretical [45] and simulation approaches [46]. Assuming an Arrhenius-like equation for the rate of diffusion in the lattice, $D_L = D_0 \exp(-E_a/k_BT)$, we can take D_0 as the Stokes-Einstein diffusion coefficient for our colloidal particles ($D_0 = 1.4 \times 10^{-1}$ $\mu m^2\,s^{-1}$, which is the expected [43] two orders of magnitude higher than our lattice diffusion), and therefore find E_a. We estimate $E_a \approx 4.5k_BT$, which is in line with the values for particle diffusion in the lattice for comparable hard-sphere colloidal crystals [46] and thus validates our measurement of D_L. Finally, from the intercept: using the fact that in the Read-Shockley equation $A = 1 + \ln a_0/2\pi r_0$ [36], where r_0 is the dislocation core radius [5], we measure a value of $A = 0.656$, which leads to $a_0/r_0 = 4.40$, consistent with values previously measured in colloidal crystals [47,48].

B. Contribution of grain rotation to grain growth

Next we briefly and qualitatively discuss the relative contribution of grain rotation to the overall rate of grain growth in the colloidal polycrystals. Rotation-induced grain growth occurs when a grain rotates to coalescence with a neighboring grain, whereas motion of the grain boundaries perpendicular to their profile serves to reduce the curvature, and thereby energy, of the boundaries [4,49]. First, we establish whether there is a coupling between these two mechanisms by plotting a two-dimensional (2D) histogram of the angular velocity, ω, versus the rate of change in the number of particles in the grain, dn/dt, as shown in Fig. 3. It is observed that the distribution is symmetric in both axes with no skew, and has a Pearson correlation coefficient of $\rho_{X,Y} = 0.018$. Therefore, there appears to be no correlation between the rotational velocity and change in grain size, which suggests there is no significant coupling between rotation-mediated and curvature-driven grain growth. As a result, we can separate the two mechanisms and combine them into a single growth law for the grain size R as follows:

$$\frac{dR}{dt} = \left(\frac{dR}{dt}\right)_{\text{curv}} + \left(\frac{dR}{dt}\right)_{\text{rot}}, \tag{5}$$

where curv and rot denote contributions from curvature- and rotation-driven grain growth, respectively.

In principle, this may suggest that curvature- and rotation-driven growth could have equal importance with respect to grain growth, however in our experiments we find this not to be the case. Grain growth in our system has been successfully described with only curvature driven growth accounted for Ref. [31], which suggests that the contribution of grain-rotation-induced coalescence is only minor in our system. This is illustrated by the following example: a grain with a diameter of $4a_0$ and a misorientation of 1° would coalesce via grain rotation in $\approx 20t_B$.

As the rotation rate is found to be independent of the (low) impurity concentration used here, we compare this to the curvature (κ) driven rate in an impurity-free GB estimated using the Herring relation for linear GB velocity, $v = M\Gamma\kappa$ [4]. Using experimental values for the GB stiffness, Γ and mobility, M [38], a grain with a diameter of $4a_0$ would disappear in $\approx 1t_B$, i.e., much faster than via grain rotation (despite the small grain size and misorientation). We note, however, that at impurity concentrations higher than in our experiments, the rate of curvature driven growth may be slower than rotation, due to Zener pinning. Additionally, rotation driven grain growth may become more significant in other situations, as has been shown in atomic systems, either through a higher temperature and rate of particle diffusion [13,21,22,50] or an increase in torque, e.g., via an applied stress [23,28,51,52]. This may mean that rotation forms part of the mechanisms of recovery after deformation via annealing, and dynamic recrystallization at high temperatures, and strains [4]. However, given our colloidal system follows the crystallization and grain growth after the quenching of a fluid, the small contribution of rotation to grain growth is consistent with observations of atomic systems.

C. Dislocation dynamics during grain rotation

As established in Sec. III A, particle diffusion in the grain is the dominant rate-limiting mechanism for grain rotation in our system. The alternative rate-controlling process, as originally suggested by Li [13], is the motion of dislocations in the grain boundary. While the latter mechanism may not be rate limiting in our system, it is crucial to facilitate rotation to a lower misorientation, as the number density of dislocations must necessarily be reduced [5]. This is achieved by dislocations gliding towards one another and reacting [25,53]. Such behavior has been observed in a colloidal polycrystal under shear [28], with dislocations gliding cross-grain, perpendicular to the boundary, to annihilate on the opposite side. In spite of this, recent work on atomic systems [54] has shown rotations at tilt boundaries (such as those in our system) can occur with dislocation glide and reactions along the boundary itself, resulting in little change in the shape of the boundary. In this work they also follow dislocation

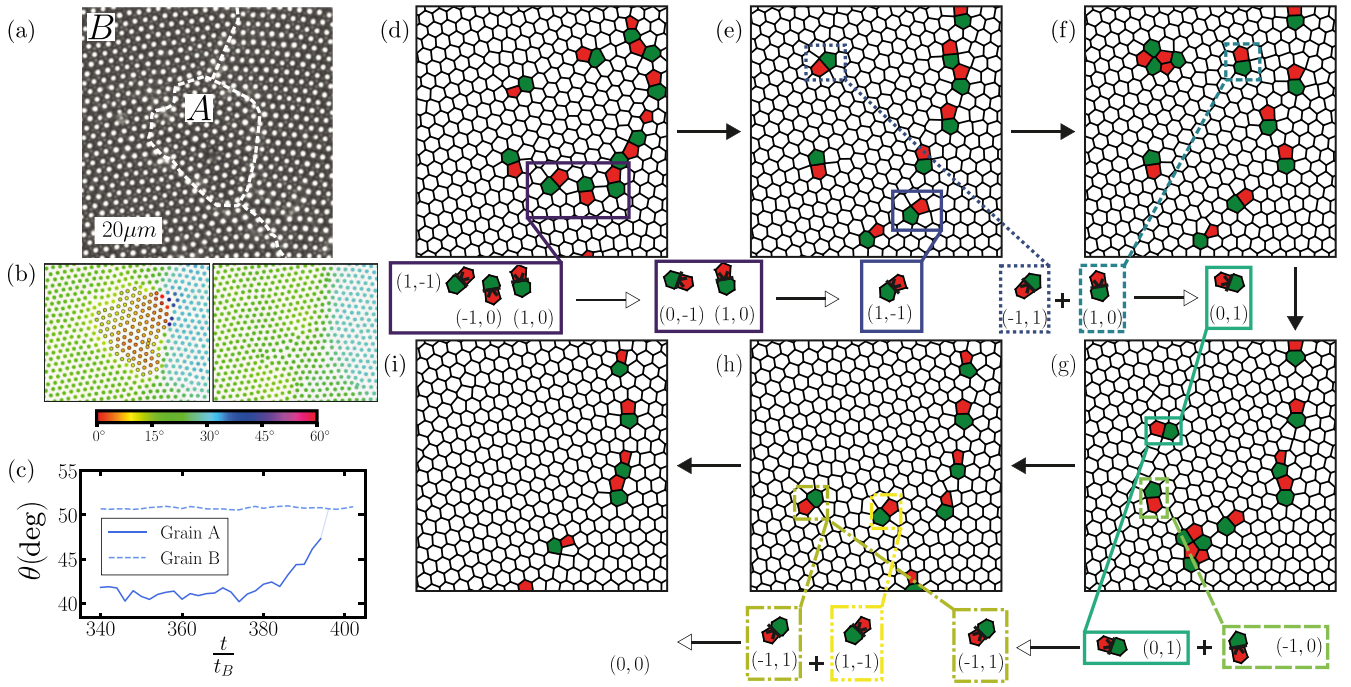

FIG. 4. Rotation to coalescence of a single grain during coarsening. (a) Microscopy images of a small grain A, which rotates to coalesce with a larger adjacent grain B. (b) Particle coordinates from panel (a) colored by orientation (see key) with grain boundaries drawn in black. The left image is before rotation, the right shows the same field-of-view after grains A and B have coalesced. (c) The orientations of grains A and B over time (scaled by the particles' Brownian time t_B), showing grain A's rotation to coalescence. (d)–(i) Voronoi constructions during the coalescence process with five- and seven-coordinate particles represented in red and green, respectively. Dislocation reactions with associated Burgers vectors are highlighted with boxes below the corresponding snapshots.

reactions via simulations, where they note that triple junctions effectively act as sinks, similar to previous simulations [32]. Despite the fact that particle diffusion in the lattice is the rate-limiting mechanism in our system, we do observe rare yet noteworthy instances of small grains rapidly rotating to coalescence. During this process, the dislocation density must be reduced through dislocations gliding and reacting, hence these rare occurrences provide a perfect opportunity to experimentally follow dislocation reactions and the role of triple junctions in a grain that rotates to coalescence.

We now study the rotation to coalescence of a small grain. These instances are unusual in terms of their relatively fast rate of rotation. However, because of this increase in angular motion, the relative timescales of the two rate-limiting mechanisms are much closer and we can clearly observe dislocation motion and reactions during coalescence. An example of this small grain rotation to coalescence is shown in Fig. 4(a), where grain A coalesces with grain B, as is also evident from the orientation plots in Figs. 4(b) and 4(c). Note that the small size ($\approx 5a_0$) and the fact that both the left and right grain boundaries' misorientations are lowered by an anticlockwise rotation, make this particular grain highly receptive to grain rotation. Interestingly, the particles in grain A move collectively (see Appendix), in stark contrast with the diffusive motion we suppose in Sec. III A. Such motion, coupled with the sudden start to rotation [seen in Fig. 4(c) at $\approx 370 t_B$], indicates a relaxation of some elastic energy. This may even be a fingerprint of grain sliding, as Gifkins [55] notes: during the sliding process, dislocations can accumulate at the triple-junctions, causing a buildup of stress, which is then subsequently relieved by the rotation of the grain and the gliding and reactions of dislocations along the boundary.

We do indeed find this particular dislocation motion, with the gliding and reactions associated with the rotation shown in Figs. 4(d)–4(i). These are Voronoi constructions of the particle coordinates at points during the coalescence, with cells colored by the number of neighboring particles (6-white, 5-red, and 7-green). The 5,7 coordinate pairs constituting dislocations sit along the grain boundaries with their orientation defined by one of six Burgers vectors. These have a magnitude of one and are defined by a hexagonal coordinate system (a, b) which is restricted to a and b being equal to -1, 0, or 1. Figures 4(d)–4(i) are a time series, showing the progression of dislocation gliding and reactions during the process of rotation of grain A. Highlighted in boxes and underneath each figure are the important dislocations (labeled with their Burgers vector) that are involved in and produced by reactions.

The first reaction occurs in Fig. 4(d) at the bottom-most triple junction, with three dislocations combining. Next, from Figs. 4(e)–4(f), a dislocation from the top-most triple junction glides along the grain boundary, and reacts with a dislocation in the A-B boundary. The produced dislocation continues this anticlockwise motion along the A-B boundary from

Figs. 4(g)–4(h). Finally, a dislocation from the bottom-most triple junction glides out, along the boundary, to annihilate with the final dislocation between A and B, leading to a total Burgers vector of (0,0) and no overall grain boundary. From this, we surmise that the grain rotation in our system occurs with dislocations gliding parallel to the grain boundary, and that the triple junctions are of key importance to this, acting as reaction sites for reactions, and are hence rendered as sources and sinks [32,54,56] for dislocations.

IV. CONCLUSIONS

Overall, we have studied the rate, role, and mechanism of grain rotation during coarsening in an impurity-doped two-dimensional colloidal polycrystal. We find the rate of rotation to be inversely proportional to the grain size and independent of the impurity concentration. This indicates that the rate-limiting mechanism is the diffusion of particles in the lattice, which we rationalize by comparing our measurements to an expression for the angular velocity of grain rotation based on diffusion-accommodated grain-boundary sliding. We contextualise the contribution of rotation-induced coalescence to grain growth, showing that rotation is independent of curvature-driven growth, which is highly dominant under our experimental conditions. We note the existence of rare elastically driven rotation events, utilizing their presence to examine the dislocation reactions associated with grain-rotation-induced coalescence and confirm predictions that triple-junctions enable rotation by effectively acting as a sink for the dislocations.

ACKNOWLEDGMENTS

We thank François Lavergne and Berend van der Meer for their insightful discussions and for critically reading the paper. The EPSRC and the European Research Council (ERC Consolidator Grant No. 724834 OMCIDC) are acknowledged for financial support.

APPENDIX

1. A sliding circular grain

Moldovan *et al.* [20] applied Raj and Ashby's theory of diffusion-accommodated sliding [33] to rotating columnar grains. Here we apply the assumptions of Moldovan *et al.* to find an expression describing the rotation of our circular grains. Raj and Ashby describe grain-boundary sliding due to an applied shear stress $\mathcal{T}$ in the y direction along a boundary whose shape is described by a cosine Fourier series:

$$x = \sum_{n=1}^{\infty} h_n \cos \frac{2\pi}{\lambda} ny, \tag{A1}$$

where h_n is the magnitude of the mode and λ is the wavelength. The diffusion-controlled sliding rate U is found to be [33]

$$U = \frac{2}{\pi} \frac{\mathcal{T}\Omega}{k_B T} \frac{\lambda}{h^2} D_L \left(\sum_{n=1}^{\infty} \left\{ \frac{\frac{h_n^2}{h^2}}{\left(1 + \frac{n\pi\delta}{\lambda} \frac{D_{GB}^{\perp}}{D_L}\right)} \right\} \right)^{-1}, \tag{A2}$$

where Ω is the atomic volume, δ is the width of the boundary, and D_L and $D_{GB}^{\perp}$ are the diffusion constants through the lattice and across the grain boundary, respectively. Specifically, $D_{GB}^{\perp}$ quantizes the rate of diffusion of a particle moving from one grain to another across the grain boundary. This is analogous to the perpendicular diffusion of the grain boundary [38], rather than the supercooled-like diffusion of particles parallel to, and within large-angle grain boundaries [57,58].

In this case, we truncate the Fourier series at the first term, as the thermal fluctuations of the boundaries are large enough that roughness is averaged out [38], hence $h_1 = h/2$ and $h_{n\neq 1} = 0$. As our grains are circular and therefore periodic, we approximate the wavelength as the length of the boundary $\lambda = 2\pi R$. Therefore, Eq. (A2) simplifies to

$$U = 16 \frac{\mathcal{T}\Omega}{k_B T} \frac{R}{h^2} D_L \left\{ 1 + \frac{\delta}{2R} \frac{D_{GB}^{\perp}}{D_L} \right\}. \tag{A3}$$

The linear velocity is related to the rotational velocity: $U = \omega R$, and the stress being the force per unit length (in 2D) is $\mathcal{T} = \tau/2\pi R^2$, as the force is τ/R. Assuming the shape of the boundary to be independent of the grain size [31], we take the amplitude of grain-boundary fluctuations to be on the order of the lattice spacing [38], hence $h \approx a_0$. The atomic volume is $\Omega = \pi a_0^2/4$. Combining this with Eq. (A3) leads to

$$\omega = \frac{2\tau}{k_B T R^2} D_L \left\{ 1 + \frac{\delta}{2R} \frac{D_{GB}^{\perp}}{D_L} \right\}. \tag{A4}$$

Experimentally we find that $\omega \propto \tau/R^2$, which implies that $1 \gg (\delta/2R)(D_{GB}^{\perp}/D_L)$, meaning lattice based diffusion D_L dominates and we find

$$\omega = \frac{2\tau}{k_B T R^2} D_L. \tag{A5}$$

We can rationalize the observation that $1 \gg (\delta/2R)(D_{GB}^{\perp}/D_L)$ as follows: From our measurements we find that $D_L = 1.1 \times 10^{-3}$ $\mu m^2\,s^{-1}$ (Sec. III A), and from Skinner *et al.* [38], who studied a very similar colloidal system, we infer that $D_{GB}^{\perp} = 1.0 \times 10^{-3}$ $\mu m^2\,s^{-1}$. While this is very similar to the lattice diffusion coefficient, the importance of perpendicular GB diffusion also depends on the ratio of the grain-boundary width to the grain radius. From the mean-square grain-boundary width of Skinner *et al.* [38], we find a boundary width of $\delta = 0.80 a_0$. From our previous work [31], we find the average grain sizes for different impurity concentrations to vary from $5a_0$ to $18a_0$, meaning the width to radius ratio is small. Hence, for our system $0.020 \leqslant (\delta/2R)(D_{GB}^{\perp}/D_L) \leqslant 0.073$, which is indeed much smaller than unity, consistent with our experimental observations.

2. Particle trajectories during rotation

In Fig. 5, we show a zoomed-in image of the particle trajectories, with an overlay of the lattice of grain B (open black circles) and the lattice of grain A (closed red circles). The particles in grain A move from their initial positions on the red circles to their final positions in the closest black circle leading to an effective rotational motion. This

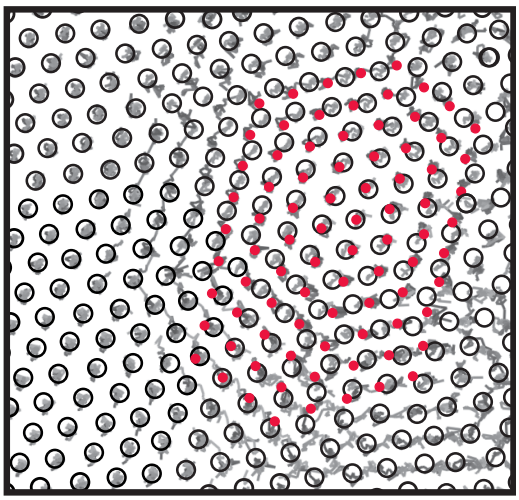

FIG. 5. The trajectories in the background in grayscale, with the lattice of grain B as black open circles and the lattice of grain A as red closed circles.

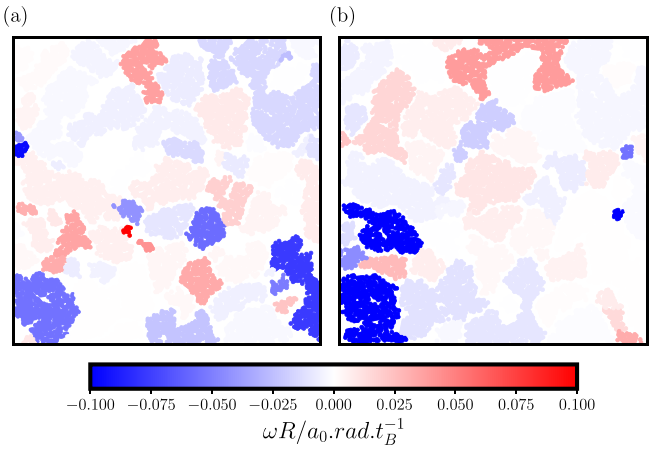

FIG. 7. Snapshots of the positions of particles colored by their grain's angular velocity, scaled by grain size. These are for a single experiment with a low impurity concentration (a) at $200t_B$ and (b) at $800t_B$.

motion is achieved as a collective, with all particles moving directly to their new lattice sites showing little diffusive motion.

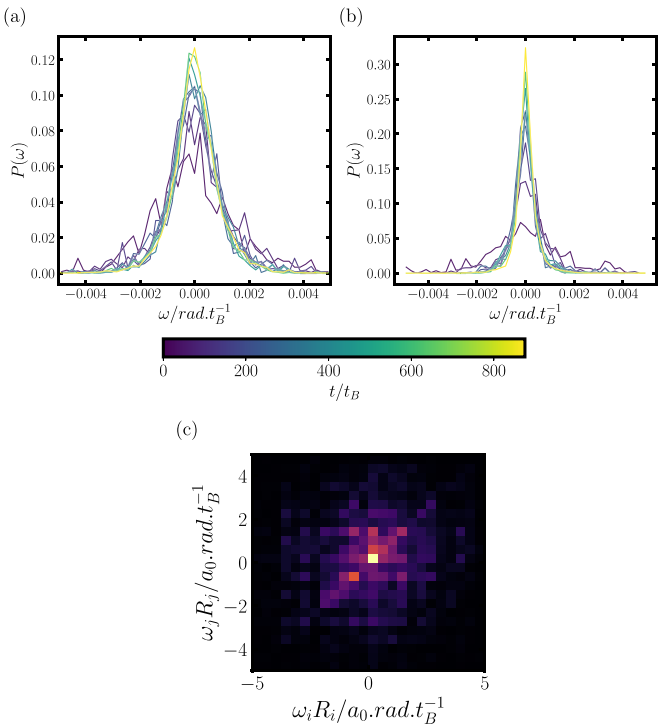

FIG. 6. (a), (b) Probability distributions of angular velocity at high ($\phi_i = 0.114$) and low ($\phi_i = 0.005$) impurity concentrations, respectively. Each line represents a different time interval, whose edges are [0,50,100,150,200,250,300,400,500,750,1000], referenced in the color bar. (c) A two-dimensional histogram, testing correlations between neighboring grains' angular velocities, $\omega_{i,j}$, normalized for their respective grain size $R_{i,j}$.

3. Chirality in grain rotation

Here, we examine the possibility of chirality playing a role in grain rotation. To this end, we measure the probability distribution of angular velocities in a single experiment, differentiating between clockwise (+) and anticlockwise (−) motion. In Figs. 6(a) and 6(b), we plot this for high ($\phi_i = 0.114$) and low ($\phi_i = 0.005$) impurity concentrations, respectively, at sequential times during the coarsening process. Irrespective of ϕ_i, we see a consistent balance between clockwise and anticlockwise angular velocities, which implies that overall there is no chirality in grain rotation in our system. As each grain begins with a random orientation, the grain-boundary orientations and thereby the torques acting on each grain are also random, hence a symmetric angular velocity distribution is expected. Note that, in our previous work [31], we found there to be no change in the distribution of grain-boundary orientations over time, so we do not expect the emergence of chirality over time either.

We furthermore analyzed the correlations between the angular velocities of neighboring grains by comparing the angular velocity of each grain, i to that of one of its neighbors, j. Using the fact that $\omega \propto 1/R$, we multiply the angular velocity by the radius to normalize for the grain size. In Fig. 6(c), we plot a two-dimensional histogram of $\omega_i R_i$ vs $\omega_j R_j$ to examine the correlations and find that there is little skew or asymmetry about the axes, implying that there is not much correlation. This is further quantified by calculating the Pearson correlation coefficient $\rho_{XY} = 0.081$, which is far from unity and close zero, indicating no local correlation between angular velocities of neighboring grains. To visualize this, we plot the positions of grains in Fig. 7, colored by their size scaled angular velocities, at times $t = 200t_B$ [Fig. 7(a)] and $800t_B$ [Fig. 7(b)]. The fact that there is no apparent spatial ordering to the direction of rotation at either time and that most of the grains have evolved to a reach different angular velocity between the two times corroborates the lack of local angular velocity correlations.

[1] J. M. Catchmark, S. Subramanian, and A. Sen, Small **1**, 202 (2005).

[2] J. Yoshioka, F. Ito, Y. Suzuki, H. Takahashi, H. Takizawa, and Y. Tabe, Soft Matter **10**, 5869 (2014).

[3] H. C. Berg, Annu. Rev. Biochem. **72**, 19 (2003).

[4] A. Rollett, F. Humphreys, G. S. Rohrer, and M. Hatherly, *Recrystallzation and Related Annealing Phenomena*, 2nd. ed. (Pergamon, Oxford, 2004).

[5] P. M. Anderson, J. P. Hirth, and J. Lothe, *Theory of Dislocations* (Cambridge University Press, Cambridge, 2017).

[6] D. Moldovan, V. Yamakov, D. Wolf, and S. R. Phillpot, Phys. Rev. Lett. **89**, 206101 (2002).

[7] L. J. Moore, R. D. Dear, M. D. Summers, R. P. A. Dullens, and G. A. D. Ritchie, Nano Lett. **10**, 4266 (2010).

[8] E. R. Leite, T. R. Giraldi, F. M. Pontes, E. Longo, A. Beltrán, and J. Andrés, Appl. Phys. Lett. **83**, 1566 (2003).

[9] K. E. Harris, V. V. Singh, and A. G. King, Acta Mater. **46**, 2623 (1998).

[10] C. S. Nichols, C. M. Mansuri, S. J. Townsend, and D. A. Smith, Acta Metall. Mater. **41**, 1861 (1993).

[11] L. Margulies, G. Winther, and H. F. Poulsen, Science **291**, 2392 (2001).

[12] Y. B. Wang, B. Q. Li, and M. L. Sui, Appl. Phys. Lett. **92**, 011903 (2008).

[13] J. C. M. Li, J. Appl. Phys. **33**, 2958 (1962).

[14] J. M. Dake, J. Oddershede, H. O. Sørensen, T. Werz, J. C. Shatto, K. Uesugi, S. Scmidt, and C. E. Krill III, Proc. Natl. Acad. Sci. USA **113**, E5998 (2016).

[15] E. Arzt, M. F. Ashby, and R. Verrall, Acta. Metall. **31**, 1977 (1983).

[16] A. Adland, Y. Xu, and A. Karma, Phys. Rev. Lett. **110**, 265504 (2013).

[17] D. A. Vega, C. K. Harrison, D. E. Angelescu, M. L. Trawick, D. A. Huse, P. M. Chaikin, and R. A. Register, Phys. Rev. E **71**, 061803 (2005).

[18] S. V. Bobylev, N. F. Morozov, and I. A. Ovid'ko, Phys. Rev. Lett. **105**, 055504 (2010).

[19] R. Ahluwalia, T. Lookman, and A. Saxena, Phys. Rev. Lett. **91**, 055501 (2003).

[20] D. Moldovan, D. Wolf, and S. R. Phillpot, Acta Mater. **49**, 3521 (2001).

[21] F. R. N. Nabarro, Philos. Mag. (1798–1977) **16**, 231 (1967).

[22] T. G. Nieh, J. Wadsworth, and O. D. Sherby, *Superplasticity in Metals and Ceramics* (Cambridge University Press, Cambridge, 1997).

[23] L. Wang, J. Teng, P. Liu, A. Hirata, E. Ma, Z. Zhang, M. Chen, and X. Han, Nat. Commun. **5**, 4402 (2014).

[24] P. Misra, *Physics of Condensed Matter* (Academic Press, Amsterdam, 2011).

[25] F. A. Lavergne, A. Curran, D. G. A. L. Aarts, and R. P. A. Dullens, Proc. Natl. Acad. Sci. USA **115**, 6922 (2018).

[26] Z. Guo and J. T. Kindt, J. Chem. Phys. **151**, 084505 (2019).

[27] F. A. Lavergne, A. Curran, D. G. A. L. Aarts, and R. P. A. Dullens, Eur. Phys. J. B **92**, 142 (2019).

[28] W. Li, Y. Peng, Y. Zhang, T. Still, A. G. Yodh, and Y. Han, Proc. Natl. Acad. Sci. USA **117**, 24055 (2020).

[29] A. R. Barth, M. H. Martinez, C. E. Payne, C. G. Couto, I. J. Quintas, I. Soncharoen, N. M. Brown, E. J. Weissler, and S. J. Gerbode, Phys. Rev. E **104**, L052601 (2021).

[30] F. A. Lavergne, S. Diana, D. G. A. L. Aarts, and R. P. A. Dullens, Langmuir **32**, 12716 (2016).

[31] J. D. Hutchinson, F. A. Lavergne, and R. P. A. Dullens, Phys. Rev. Mater. **6**, 075604 (2022).

[32] K. Wu and P. W. Vorhees, Acta Mater. **60**, 407 (2012).

[33] R. Raj and M. F. Ashby, Metall. Trans. **2**, 1113 (1971).

[34] F. A. Lavergne, D. G. A. L. Aarts, and R. P. A. Dullens, Phys. Rev. X **7**, 041064 (2017).

[35] J. C. Crocker and D. G. Grier, J. Colloid Interface Sci. **179**, 298 (1996).

[36] W. T. Read and W. Shockley, Phys. Rev. **78**, 275 (1950).

[37] M. Upmanyu, D. J. Srolovitz, A. E. Lobkovskyc, J. A. Warren, and W. C. Carter, Acta Mater. **54**, 1707 (2006).

[38] T. O. E. Skinner, D. G. A. L. Aarts, and R. P. A. Dullens, Phys. Rev. Lett. **105**, 168301 (2010).

[39] D. Frenkel and A. J. C. Ladd, Phys. Rev. Lett. **59**, 1169 (1987).

[40] R. P. A. Dullens and C. Bechinger, Phys. Rev. Lett. **107**, 138301 (2011).

[41] A. Pertsinidis and X. S. Ling, Nature (London) **413**, 147 (2001).

[42] R. Laghaei, S. A. Asher, and R. D. Coalson, J. Phys. Chem. B **117**, 5271 (2013).

[43] S. Pronk and D. Frenkel, J. Chem. Phys. **110**, 4589 (1999).

[44] F. Smallenburg, L. Filion, M. Marechal, and M. Dijkstra, Proc. Natl. Acad. Sci. USA **109**, 17886 (2012).

[45] P. Heitjans and J. Kärger, *Diffusion in Condensed Matter: Methods, Materials, Models* (Springer, Heidelberg, 2005).

[46] B. van der Meer, M. Dijkstra, and L. Filion, J. Chem. Phys. **146**, 244905 (2017).

[47] M. Jorand, F. Rothen, and P. Pieranski, J. Phys. Colloq. **46**, C3-245 (1985).

[48] P. Schall, I. Cohen, D. A. Weitz, and F. Spaepen, Nature (London) **440**, 319 (2006).

[49] J. W. Christian, *The Theory of Transformations in Metals and Alloys* (Pergamon, Oxford, 2002).

[50] C. Herring, J. Appl. Phys. **21**, 437 (1950).

[51] A. J. Halsam, D. Moldovan, V. Yamakov, D. Wolf, S. R. Phillpot, and H. Gleiter, Acta Mater. **51**, 2097 (2003).

[52] T. Gorkaya, K. D. Molodov, D. A. Molodov, and G. Gottstein, Acta Mater. **59**, 5674 (2011).

[53] W. T. M. Irvine, A. D. Hollingsworth, D. G. Grier, and P. M. Chaikin, Proc. Natl. Acad. Sci. USA **110**, 15544 (2013).

[54] Y. Guo, J. Teng, G. Yang, A. Li, Y. Deng, C. Yang, L. Wang, X. Yan, Z. Zhang, X. Li, E. Ma, and X. Han, Acta Mater. **241**, 118386 (2022).

[55] R. C. Gifkins, Metall. Trans. A **7**, 1225 (1976).

[56] J. W. Cahn and J. E. Taylor, Acta Mater. **52**, 4887 (2004).

[57] T. O. E. Skinner, D. G. A. L. Aarts, and R. P. A. Dullens, J. Chem. Phys. **135**, 124711 (2011).

[58] K. H. Nagamanasa, S. Gokhale, R. Ganapathy, and A. K. Sood, Proc. Natl. Acad. Sci. USA **108**, 11323 (2011).